Research on dynamic characteristics and identification method of local defect on the roll surface

Wu Shengli[a], Xing Wenting[b*], Liu Ying[c], Shao Yimin[d]

[a]*College of Traffic and Transportation, Chongqing Jiaotong University, Chongqing, 400074, People's Republic of China*

[b] *College of Management, Chongqing Technology and Business University, Chongqing 400067, People's Republic of China*

[c]*School of Engineering, Cardiff University, Cardiff, CF24 3AA, UK*

[d]*State Key Laboratory of Mechanical Transmissions, Chongqing University, Chongqing, 400044, People's Republic of China*

**Corresponding author. E-mail: cqw20141001@sina.com*

Abstract

Local defects are prone to be produced on the surface of roll during long-term work, which will not only cause abnormal vibration of the roll mill but also affect the quality of steel strip. In particular, identifying defect on the roll surface in well-lubricated state is one of the existing difficulties. The time-varying oil film stiffness model is proposed based on the elastohydrodynamic lubrication theory. A Sendzimir twenty-high roll mill model is established and combined with the time-varying oil film stiffness model to analyze the vibration characteristics of the roll mill. At the same time, a new method for real-time identification of the defect size during the rolling process is proposed. Agreement between the simulated results and the experimental results validates the effectiveness of the established model. The changes of the oil film stiffness and the roll mill vibration characteristics under different defect sizes on the roll surface are analyzed, which provides a theoretical support for the identification of the local defect on the roll surface.

Keywords：Oil film stiffness; Defect on the roll; Dynamic model of roll mill

1. Introduction

The spalling defect will occur on the roll surface inevitably under alternating stresses in the rolling process. The abnormal vibration of the roll mill is induced by using the roll with a spalling defect on the surface, which seriously degrade the surface quality of the steel strip.

Though chatter vibration is restrained to some degree by a large amount of lubricating oil between rolls, it leads more difficult to identify the local defect on the roll surface. Therefore, studying the vibration mechanism of local defects in good lubrication states helps identify the defects, and also plays an important role in dealing with the roll surface defects and improving production efficiency.

By combining high-resolution SEM with XRD data, Souza revealed the strain hardening mechanisms of the formation of submicron structural defects within austenite and martensite during the cold rolling process [1]. The mathematical model for defects of a steel strip was developed, which could be used to prevent the local defects on the steel strip [2]. Furthermore, Yu studied the characteristics and evolution of steel strip surface caused by non-metallic inclusions generated in steelmaking and casting process, which will help to take timely measures to improve the steel strip surface quality [3]. In the research of roll surface defects, more attention has been paid to the mechanism of roll surface defects. The research results of Deng showed that the surface oxidation of the roll caused tensile residual stress on the substrate and compressive stress on the oxide layer [4]. Due to the exfoliation of carbides on the grain boundaries, micro-voids were formed on the surface of the work roll. These micro-voids could act as initiation sites of cracks during further cyclic heating and cooling [5]. Of course, other factors affecting the surface quality of steel strip have also been studied. Moazeni studied the causes of formation of shape defects in flat rolling product, the results showed that the nonuniform deformation along the plate width leaded to formation of longitudinal stress [6].

Lubricating oil between the rolls not only can help to reduce friction between the rolls but

also reduces the temperature of the roll mill. The type of lubrication between rolls was identified as the cause of the vibration [7]. But a good lubrication system also can help to improve the stability of the mill during high-speed rolling and improve rolling efficiency [8]. Wilson proposed a formula for calculating the oil film thickness of a roll mill under good lubrication conditions [9]. Subsequently, Reich's research showed that under the condition of poor lubrication, the oil film thickness was less affected by the rolling speed during high-speed rolling [10]. Meanwhile researchers paid more focus on oil film research, different oil film calculation models and the influence of rolling parameters on oil film thickness in the deformation zone of the rolling mill were analyzed [11, 12].

Although the mechanism of roll surface defects and the oil film models have been studied, it is difficult to identify the roll surface defects in time due to multiple interface contacts between the rolls [13]. Therefore in the present paper, the oil film stiffness of the local defect on the roll surface will be studied based on elastohydrodynamic lubrication theory, the twenty-high roll mill dynamic model is established to analyze the corresponding characteristics. Meanwhile, an adaptive wavelet will be used to identify the size of the roll surface defect, which provides a theoretical support for the identification of the roll local defect and the evolution mechanism of the defect in the black box condition.

2. Time-varying film stiffness between two rolls under elastohydrodynamic lubrication

2.1 The change process of film stiffness

During the rolling process, under high alternating pressure and high-temperature conditions,

initial cracks will form on the roll surface. As the number of contact cycles increases, initial cracks will gradually develop defects such as spalling [14]. The local defect on the roll surface is shown in Figure 1. A large amount of lubricant is used to reduce friction and temperature in the roll system during the rolling process. As the rolling speed increases, oil films will be formed between the rolls and between the working roll and the steel strip. The oil film between normal rolls and the oil film between defective roll and normal roll are shown in Figure 2.

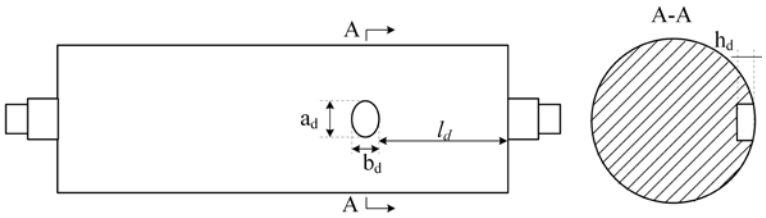

Fig. 1 Sketch of the local defect on the roll

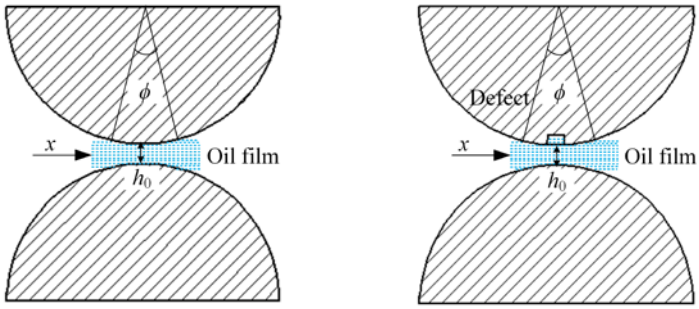

(a) Normal rolls (b) Defective roll

Fig. 2 Sketch of the process of rolls contact

Figure 3 shows the change of oil film stiffness. Lines Ⅰ, Ⅱ and Ⅲ indicate that the defect width is less, equal to and greater than the oil film width of the contact area. Pink, yellow and black indicate that the defect is about to enter the oil film area, in the oil film area and out of the oil area respectively. Oil film stiffness decreases as the defect enters the oil film area, as shown at $Ⅰ_a$, $Ⅱ_b$ and $Ⅲ_c$. Of course, oil film stiffness will increase as the defect leaves the oil film area, as shown at $Ⅰ_{a''}$, $Ⅱ_{b''}$ and $Ⅲ_{c''}$. When the defect width is smaller and greater

than the width of the oil film in the contact area, the defect will remain constant in the oil film area for a certain period with the roll rotation, so the oil film stiffness will remain constant, as shown at Ⅰ$_{a'}$ and Ⅲ$_{c'}$.

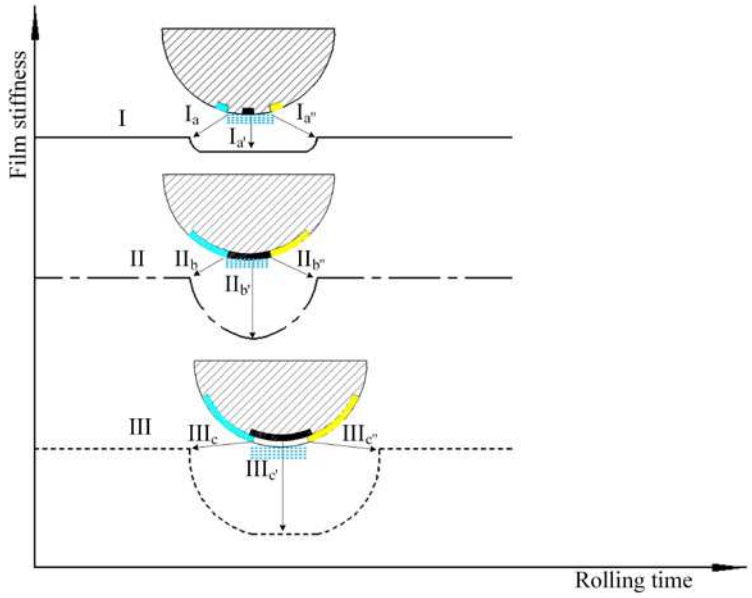

Fig. 3 Variation of the film stiffness

2.2 Film stiffness calculation

According to the theory of elastohydrodynamic lubrication, the unit oil film pressure can be expressed as [15]

$$\frac{\mathrm{d}p}{\mathrm{d}x} = 6\eta u \frac{h - h_0}{h^3} \tag{1}$$

Where p is the unit oil film pressure，η is the dynamic viscosity of lubricating fluid，u is the entrainment velocity，h is the oil film thickness in the contact area，and h_0 is the minimum oil film thickness, h_0 can be obtained by Dawson-Higginson formula [16]

$$h_0 = 2.65\kappa^{0.54}(\eta u)^{0.7} R^{0.43} E'^{-0.03} W^{-0.13} \tag{2}$$

Where κ is the viscosity coefficient, W is the normal load per unit length, E' is the equivalent elastic Young's modulus.

$$\frac{1}{E'}=\frac{1}{2}\left[\frac{1-\upsilon_1^2}{E_1}+\frac{1-\upsilon_2^2}{E_2}\right] \tag{3}$$

υ_1 and υ_2 are the Poisson's ratios of rolls respectively, E_1 and E_2 are the elastic Young's modulus of rolls respectively.

Equation 1 can be converted into polar coordinates, substitute $dx = Rd\phi$ and $u = R\omega$ into Equation 1. Equation 1 can be expressed as

$$\frac{dp}{d\phi}=\frac{6\eta R^2\omega}{\left(h_0+R\left(1-\cos\phi\right)\right)^3}\left(R(1-\cos\phi)\right) \tag{4}$$

R is the equivalent radius of curvature，where $R = R_1R_2/(R_1+R_2)$，ϕ is the oil film angle, as shown in Fig. 2, ω is the angular velocity.

$$p_\phi = 6\eta R^2\omega\int_{\phi_1}^{\phi_2}\frac{R(1-\cos\phi)}{(h_0+R(1-\cos\phi))^3}d\phi \tag{5}$$

Therefore the oil film force on the roll can be expressed as

$$F=\int_{-\frac{L}{2}}^{\frac{L}{2}}\int_{\phi_1}^{\phi_2} p_\phi RdLd\phi \tag{6}$$

Where L is the contact length.

The film stiffness and film damping can be obtained by formula 7 and formula 8 respectively [17].

$$k=\frac{\partial F}{\partial x} \tag{7}$$

$$c=\frac{\partial F}{\partial u} \tag{8}$$

3. Twenty-high roll mill dynamic model coupling vertical and horizontal vibrations

The structure of the Sendzimir twenty-high roll mill is symmetrical, and the upper-half part is taken into the study as shown in Fig. 4. No.1 roll is the working roll. No.2 and No.3 roll are

the first intermediate rolls. No.4, No.5 and No.6 are the second intermediate rolls. No.4, No.5 and No.6 are the support rolls.

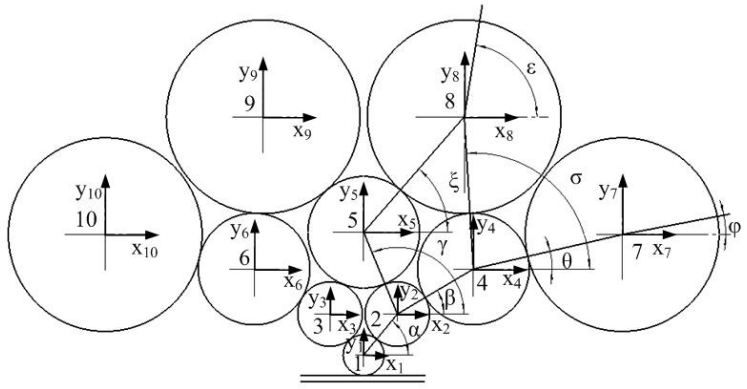

Fig. 4 Sketch of the position of the Sendzimir cluster mill [18]

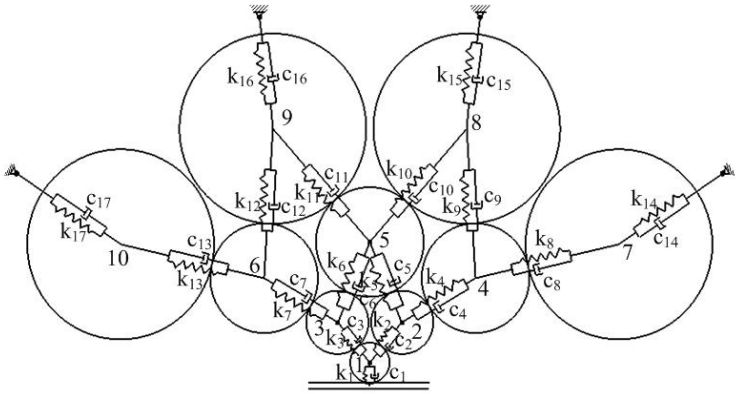

Fig. 5 Sketch of the Sendzimir cluster mill analyzed

y_i , $\dot{y}_i$ and $\ddot{y}_i$ stand for displacement, velocity and acceleration respectively, where $i = 1, 2 \cdots 10$. k_i is the film stiffness and c_i is the damping, as shown in Fig. 5. m_i represents the mass of different rolls. Therefore the dynamic model of vertical vibration of ten-degree-of-freedom rolling mill is as follows:

$$\begin{aligned} &m_1\ddot{y}_1 + \{c_2(\dot{y}_1 - \dot{y}_2) + k_2(y_1 - y_2)\}\sin^2\alpha \\ &+\{c_3(\dot{y}_1 - \dot{y}_3) + k_3(y_1 - y_3)\}\sin^2(\pi - \alpha) = F - k_1 y_1 - c_1\dot{y}_1 \end{aligned} \tag{9}$$

$$\begin{aligned} &m_2\ddot{y}_2 + \{c_4(\dot{y}_2 - \dot{y}_4) + k_4(y_2 - y_4)\}\sin^2\beta \\ &+\{c_5(\dot{y}_2 - \dot{y}_5) + k_5(y_2 - y_5)\}\sin^2\gamma \\ &-\{c_2(\dot{y}_1 - \dot{y}_2) + k_2(y_1 - y_2)\}\sin^2\alpha = 0 \end{aligned} \tag{10}$$

$$m_3\ddot{y}_3+\{c_6(\dot{y}_3-\dot{y}_5)+k_6(y_3-y_5)\}\sin^2(\pi-\gamma)$$
$$+\{c_7(\dot{y}_3-\dot{y}_6)+k_7(y_3-y_6)\}\sin^2(\pi-\beta) \quad (11)$$
$$-\{c_3(\dot{y}_1-\dot{y}_3)+k_3(y_1-y_3)\}\sin^2(\pi-\alpha)=0$$

$$m_4\ddot{y}_4+\{c_8(\dot{y}_4-\dot{y}_7)+k_8(y_4-y_7)\}\sin^2\theta$$
$$+\{c_9(\dot{y}_4-\dot{y}_8)+k_9(y_4-y_8)\}\sin^2\sigma \quad (12)$$
$$-\{c_4(\dot{y}_2-\dot{y}_4)+k_4(y_2-y_4)\}\sin^2\beta=0$$

$$m_5\ddot{y}_5+\{c_{10}(\dot{y}_5-\dot{y}_8)+k_{10}(y_5-y_8)\}\sin^2\xi$$
$$+\{c_{11}(\dot{y}_5-\dot{y}_9)+k_{11}(y_5-y_9)\}\sin^2(\pi-\xi)- \quad (13)$$
$$\{c_5(\dot{y}_2-\dot{y}_5)+k_5(y_2-y_5)\}\sin^2\gamma$$
$$-\{c_6(\dot{y}_3-\dot{y}_5)+k_6(y_3-y_5)\}\sin^2(\pi-\xi)=0$$

$$m_6\ddot{y}_6+\{c_{12}(\dot{y}_6-\dot{y}_9)+k_{12}(y_6-y_9)\}\sin^2(\pi-\sigma)$$
$$+\{c_{13}(\dot{y}_6-\dot{y}_{10})+k_{13}(y_6-y_{10})\}\sin^2(\pi-\theta) \quad (14)$$
$$-\{c_7(\dot{y}_3-\dot{y}_6)+k_7(y_3-y_6)\}\sin^2(\pi-\beta)=0$$

$$m_7\ddot{y}_7+\{c_8(\dot{y}_7-\dot{y}_4)+k_8(y_7-y_4)\}\sin^2\theta \quad (15)$$
$$+(c_{14}\dot{y}_7+k_{14}y_7)\sin^2\varphi=0$$

$$m_8\ddot{y}_8+\{c_9(\dot{y}_8-\dot{y}_4)+k_9(y_8-y_4)\}\sin^2(\pi-\sigma)$$
$$+\{c_{10}(\dot{y}_8-\dot{y}_5)+k_{10}(y_8-y_5)\}\sin^2\xi \quad (16)$$
$$+(c_{15}\dot{y}_8+k_{15}y_8)\sin^2\varepsilon=0$$

$$m_9\ddot{y}_9+\{c_{12}(\dot{y}_9-\dot{y}_6)+k_{12}(y_9-y_6)\}\sin^2(\pi-\sigma)$$
$$+\{c_{11}(\dot{y}_9-\dot{y}_5)+k_{11}(y_9-y_5)\}\sin^2\xi \quad (17)$$
$$+(c_{16}\dot{y}_9+k_{16}y_9)\sin^2\varepsilon=0$$

$$m_{10}\ddot{y}_{10}+\{c_{13}(\dot{y}_{10}-\dot{y}_6)+k_{13}(y_{10}-y_6)\}\sin^2\theta \quad (18)$$
$$+(c_{17}\dot{y}_{10}+k_{17}y_{10})\sin^2\varphi=0$$

4 Discussion on simulation results

4.1 Parameters of simulation

The diameter of the support roll $D_7=D_8=D_9=D_{10}$=300 mm, the diameter of the second intermediate roll $D_4=D_5=D_6$=171.66 mm, the diameter of the first intermediate roll $D_2=D_3$=97.4 mm, and the other structural parameters of the roll mill are shown in Table 1.

Table 1. Parameters of the roll mill

Items	Amount

The diameter of working roll/mm	68.7
Length of working roll/mm	1440
Length of the first intermediate roll/mm	1578
Young's modulus/ GPa	218
Density/(kg/m^3)	7830

4.2 Simulation results

According to the analysis process in Fig. 3 and formula 7, the oil film stiffness between different rolls can be obtained, as shown in Fig. 6. The defect is on the surface of the No.5 roll. For different defect sizes, the change curves of the oil film stiffness between the No. 9 roll and the No. 5 roll, as shown in Fig. 6(a). Where 'Small' indicates that the size of the defect is smaller than the width of the oil film. 'Same' indicates that the size of the defect equals the width of the oil film, and 'Large' represent the defect size is bigger than the width of the oil film. Figure 6(b) shows the change curves of the oil film stiffness between the No.3 roll and the No.5 roll.

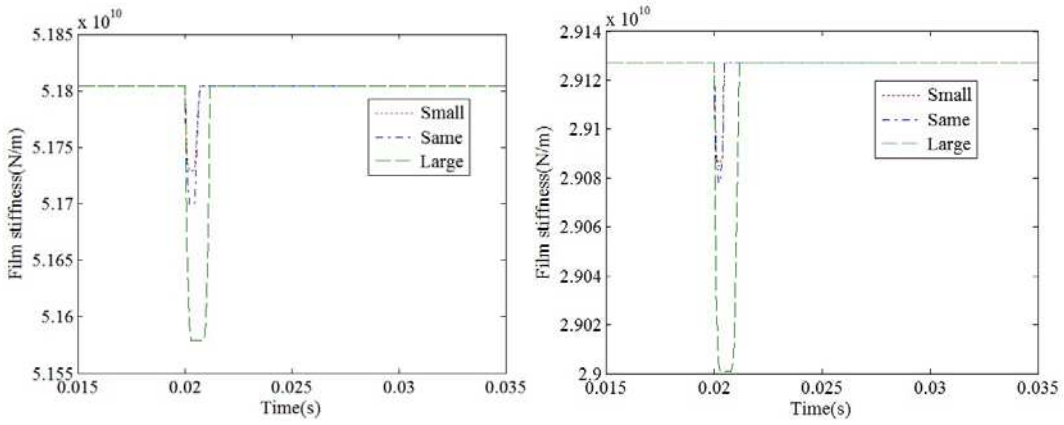

(a) The No. 5 roll and the No. 9 roll (b) The No. 5 roll and the No. 3 roll

Fig. 6 The film stiffness between different rolls

The defect size is set to 26 mm, the simulated signal and the corresponding envelope spectrum also can be obtained based on the dynamic model, as shown in Fig. 7. Periodic shocks can be seen in Fig. 7(a). Figure 7(b) shows that at a rolling speed of 300 m/min, the

characteristic frequency of the second intermediate roll is 9.155 Hz. Symbol ①, ②, ③ and ④ indicate periodic shocks.

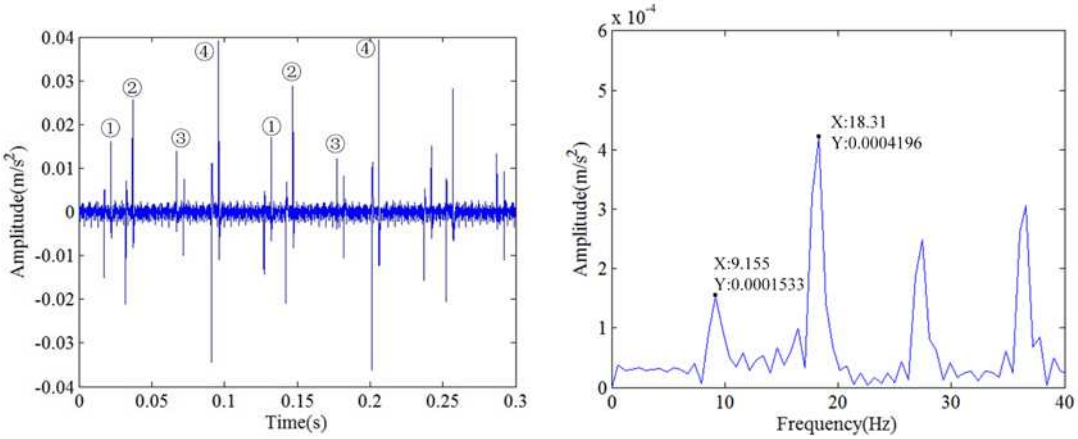

(a) Simulated signal (b) Frequency spectrum

Fig. 7 Simulated signal and the corresponding envelope spectrum

4.3 Defect size identification

The more similar the wavelet function shape to the time domain signal, the constructed adaptive wavelet can identify the duration of the defect [19]. The raw vibration signal is used to construct an adaptive wavelet function based on the MATLAB wavelet toolbox [20]. Therefore the constructed adaptive wavelet is used to identify the defect size, as shown in Fig. 8. Impact duration $t_1 = t_2 = t_3 = t_4 = t_{las}$=0.0051s, the rolling speed is 300 m/min, so the defect size is approximately equal to 25.5 mm with an accuracy of 98.08%.

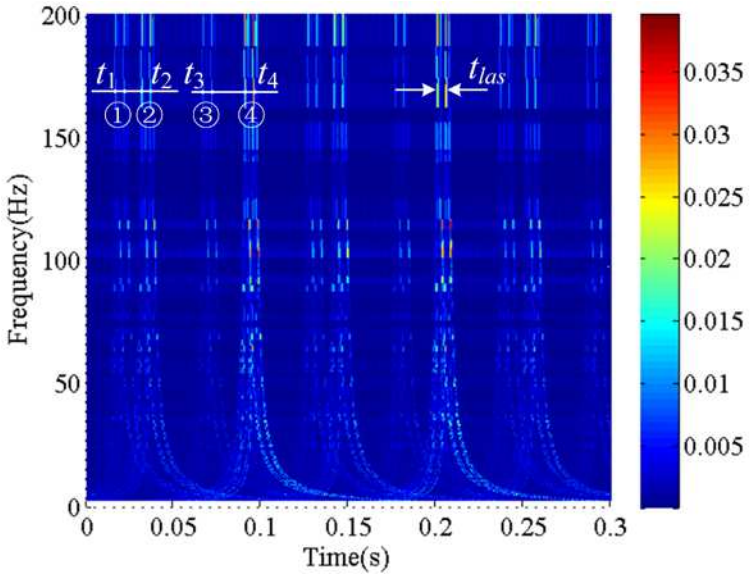

Fig. 8 The defect size identification of the simulation signal

5 Experimental verification

Rolling parameters are listed in Table 2. The defect on the surface of the No. 5 roll, as shown in Fig. 9. The defect size is about 26 mm. LMS data acquisition device and the B&K acceleration sensor were employed to obtain vibration signal. The acceleration sensor is installed on the roll mill stand near the No. 9 roll, as shown in Fig. 10. The sampling frequency is 10240 Hz.

Table 2. Parameters of the rolling process

Rolling Force/t	Rolling Speed /(m/min)	Front Tension Force/(N/mm^2)	Rear Tension Force/(N/mm^2)	Entry Thickness/ mm	Exit Thickness/ mm
590.2	300	29	28	2.7	2.5

Fig. 9 Defect on the surface of the roll

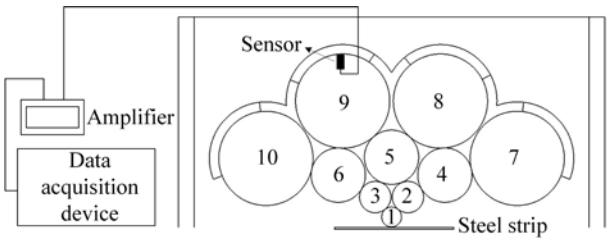

Fig.10 The experimental equipment and the location of the sensor

The measured signal and the corresponding envelope spectrum are shown in Fig. 11. Periodic shocks also can be seen in Fig. 11(a). 9.21 Hz and 18.44 Hz are the characteristic frequency and the second harmonic frequency of the No.5 roll, respectively. Consistency of experimental results and simulation results, which verifies the validity of the model.

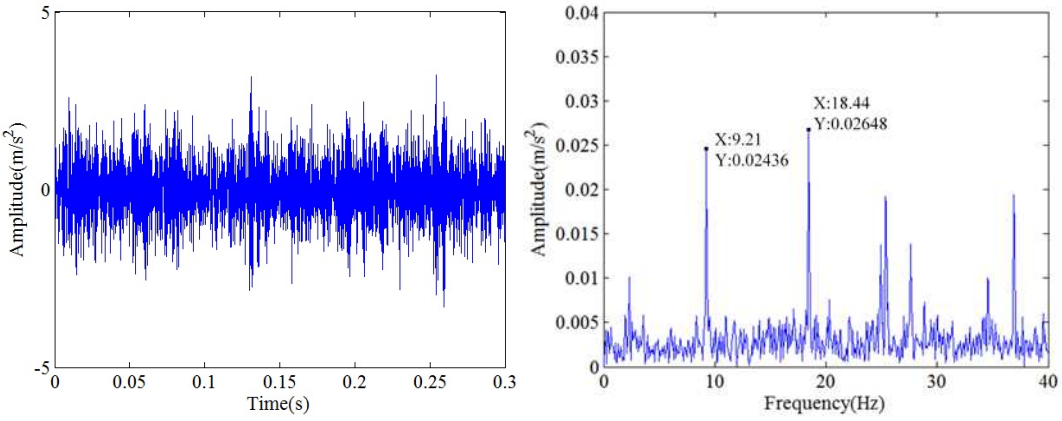

(a) Experimental signal (b) Frequency spectrum

Fig. 11 The experimental signal and the corresponding frequency spectrum

The adaptive wavelet constructed from the measured signal is used to identify the defect size, as shown in Fig. 12. Impact duration $t_{1tes} = t_{2tes} = t_{3tes}$ =0.0058s, the rolling speed is 300 m/min, so the defect size approximately equal 29 mm. The validity of the defect size identification method is verified by simulation results and experimental results.

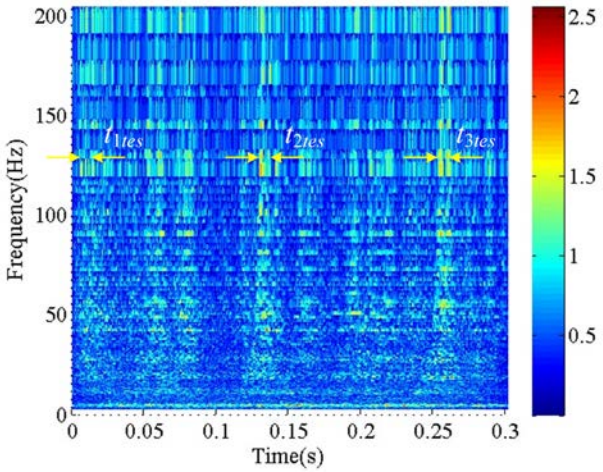

Fig. 12 The defect size identification of the experimental signal

6 Effect of defect size on vibration characteristics of rolling mill

As the defect size increases, both the amplitude of the vibration signal and the amplitude of the envelope spectrum also increase, as shown in Fig. 13.

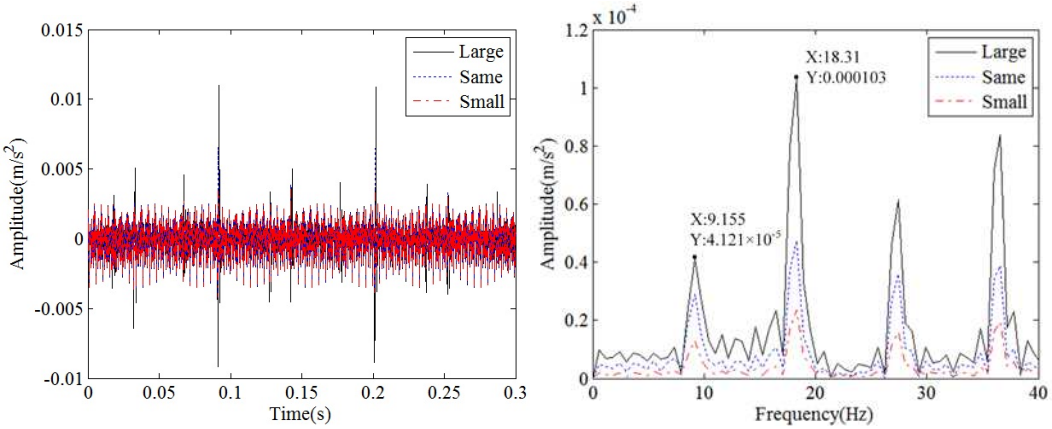

(a) Simulated signal (b) Frequency spectrum

Fig. 13 The vibration characteristics of the roll mill at different defect sizes

Figure 14 shows that the amplitude will increase very much when the defect size equal to the oil film width of the contact area. In the actual production process, in order to save costs, even the roll with a defect will continue to be used. Therefore, when small defect is found on the surface of the roll, the roll is usually polished to prevent flaking substances of the roll

surface from damaging the roll mill and the steel strip surface. The size of the defect should be larger than the width of the oil film to prevent a significant increase in vibration amplitude of the roll mill, as shown in Fig. 15.

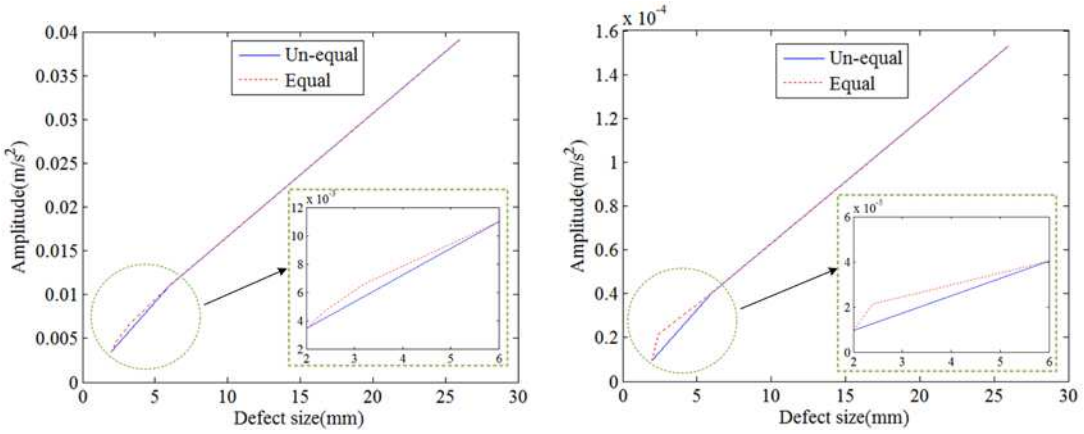

(a) Vibration amplitude (b) Amplitude of the frequency spectrum

Fig. 14 The amplitude of the roll mill

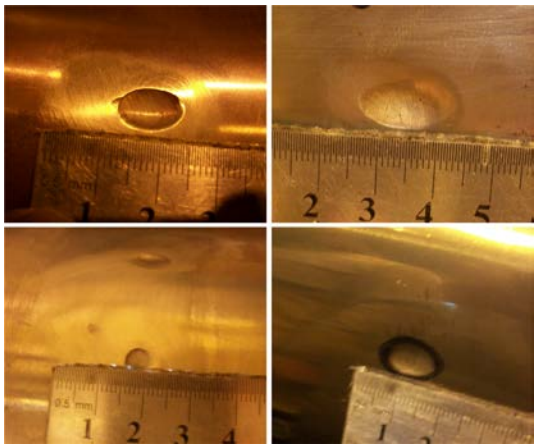

Fig. 15 Defects on the roll surface

7 Conclusion

Based on the theory of elastohydrodynamic lubrication, an oil film time-varying stiffness model is established. At the same time, the Sendzimir twenty-high roll mill dynamic model is used to analyze the vibration characteristics of the roll mill. The validity and accuracy of the

model were verified by the experimental results.

An adaptive wavelet is used to identify the defect size, which provides a practical method for detecting the defect size without stopping the roll mill. Identify small defects on the roll surface and polish the defects in time, which is beneficial to reduce the vibration amplitude of the roll mill.

Acknowledgements

The authors are grateful for the National Natural Science Foundation of China under Contract No. 51705052 and the Chongqing Education Commission Project under Contract No. KJ1705141.

References

[1] Souza Filho I R, Sandim M J R, Ponge D, et al. Strain hardening mechanisms during cold rolling of a high-Mn steel: Interplay between submicron defects and microtexture[J]. Materials Science and Engineering: A, 2019, 754: 636-649.
[2] Shatalov R, Maksimov E, Koinov T, et al. Research of flatness defects forming at 20-hi steel strips rolling mill[J]. Journal of Chemical Technology and Metallurgy, 2017, 52(2): 199-204.
[3]Yu H, Ji C, Chen B, et al. Characteristics and evolution of inclusion induced surface defects of cold rolled IF sheet[J]. Journal of Iron and Steel Research International, 2015, 22(1): 17-23.
[4]Deng G Y, Tieu A K, Su L H, et al. Microstructural study and residual stress measurement of a hot rolling work roll material during isothermal oxidation[J]. The International Journal of Advanced Manufacturing Technology, 2019, 102(5-8): 2107-2118.
[5]Deng G Y, Zhu Q, Tieu K, et al. Evolution of microstructure, temperature and stress in a high speed steel work roll during hot rolling: Experiment and modelling[J]. Journal of Materials Processing Technology, 2017, 240: 200-208.
[6]Moazeni B, Salimi M. Investigations on relations between shape defects and thickness profile variations in thin flat rolling[J]. The International Journal of Advanced Manufacturing Technology, 2015, 77(5-8): 1315-1331.
[7] Lee D K, Nam J, Kang J S, et al. Investigation of the cause of the chatter and physical behavior of a work roll in compact endless rolling[J]. The International Journal of Advanced Manufacturing Technology, 2018, 94(9-12): 4459-4467.
[8] Fujita N, Kimura Y, Kobayashi K, et al. Dynamic control of lubrication characteristics in high speed tandem cold rolling[J]. Journal of Materials Processing Technology, 2016, 229: 407-416.
[9] Wilson W R D. Friction and lubrication in bulk metal-forming processes[J]. Journal of Applied Metalworking, 1978, 1(1): 7-19.

[10] Reich R, Urbanski J. Experimental support for the dynamic concentration theory of forming an oil reservoir at the inlet of the roll bite by measuring the onset speed of starvation as a function of oil concentration and droplet size[J]. Tribology Transactions. 2004, 47: 489-499.
[11] Li X J, Cui Y Y, He Z L, et al. Model and influence factors of oil film thickness in the deformation zone of double cold reduction mill[J]. Ironmaking & Steelmaking, 2019: 1-7.
[12]Kimura Y, Fujita N, Matsubara Y, et al. High-speed rolling by hybrid-lubrication system in tandem cold rolling mills[J]. Journal of Materials Processing Technology, 2015, 216: 357-368.
[13] Xiao H, Shao Y, Xu J. Investigation into the energy dissipation of a lap joint using the one-dimensional microslip friction model[J]. European Journal of Mechanics-A/Solids, 2014, 43: 1-8.
[14] Wu Q, Sun D L, Liu C S, et al. Analysis of surface and sub-surface initiated spalling of forged cold work rolls[J]. Engineering Failure Analysis, 2008, 15(4): 401-410.
[15] Kimura Y, Sodani Y, Nishiura N, et al. Analysis of chatter in tandem cold rolling mills[J]. ISIJ international, 2003, 43(1): 77-84.
[16] Lubrecht A A, Venner C H, Colin F. Film thickness calculation in elasto-hydrodynamic lubricated line and elliptical contacts: the Dowson, Higginson, Hamrock contribution[J]. Proceedings of the Institution of Mechanical Engineers, Part J: Journal of Engineering Tribology, 2009, 223(3): 511-515.
[17]Zhang Y, Liu H, Zhu C, et al. Oil film stiffness and damping in an elastohydrodynamic lubrication line contact-vibration[J]. Journal of Mechanical Science and Technology, 2016, 30(7): 3031-3039.
[18] Brusa E, Lemma L, and Benasciutti D. Vibration analysis of a Sendzimir cold rolling mill and bearing fault detection[J]. Mechanical Engineering Science,2010, 224: 1-10.
[19] Jena D P, Panigrahi S N. Bearing and gear fault diagnosis using adaptive wavelet transform of vibration signals[J]. Procedia Engineering, 2012 (50): 265-274.
[20] Sadooghi M S, Khadem S E. A new performance evaluation scheme for jet engine vibration signal denoising[J]. Mechanical Systems and Signal Processing, 2016, 76: 201-212.